Carbon nanotubes degraded by neutrophil myeloperoxidase induce less pulmonary inflammation

Valerian E. Kagan[1,*], **Nagarjun V. Konduru**[1], **Weihong Feng**[1], **Brett L. Allen**[2], **Jennifer Conroy**[3], **Yuri Volkov**[3], **Irina I. Vlasova**[1], **Natalia A. Belikova**[1], **Naveena Yanamala**[4], **Alexander Kapralov**[1], **Yulia Y. Tyurina**[1], **Jingwen Shi**[5], **Elena R. Kisin**[6], **Ashley R. Murray**[6], **Jonathan Franks**[7], **Donna Stolz**[7], **Pingping Gou**[2], **Judith Klein-Seetharaman**[4], **Bengt Fadeel**[5], **Alexander Star**[2], **Anna A. Shvedova**[6]

[1]Department of Environmental and Occupational Health, Center for Free Radical and Antioxidant Health, Graduate School of Public Health, University of Pittsburgh, Pittsburgh, Pennsylvania, USA [2]Department of Chemistry, University of Pittsburgh, Pittsburgh, Pennsylvania, USA [3]Department of Clinical Medicine and Centre for Research on Adaptive Nanostructures and Nanodevices (CRANN), Trinity College Dublin, Dublin, Ireland [4]Department of Structural Biology, University of Pittsburgh, Pittsburgh, Pennsylvania, USA [5]Division of Molecular Toxicology, Institute of Environmental Medicine, Karolinska Institutet, Stockholm, Sweden [6]Pathology and Physiology Research Branch, Health Effects Laboratory Division (HELD), National Institute for Occupational Safety and Health (NIOSH) and Department of Physiology and Pharmacology, West Virginia University, Morgantown, West Virginia, USA [7]Department of Cell Biology and Physiology, University of Pittsburgh, Pittsburgh, Pennsylvania, USA.

Abstract

We have shown previously that single-walled carbon nanotubes can be catalytically biodegraded over several weeks by the plant-derived enzyme, horseradish peroxidase[1]. However, whether peroxidase intermediates generated inside human cells or biofluids are involved in the biodegradation of carbon nanotubes has not been explored. Here, we show that hypochlorite and reactive radical intermediates of the human neutrophil enzyme myeloperoxidase catalyse the biodegradation of single-walled carbon nanotubes *in vitro*, in neutrophils and to a lesser degree in

macrophages. Molecular modelling suggests that interactions of basic amino acids of the enzyme with the carboxyls on the carbon nanotubes position the nanotubes near the catalytic site. Importantly, the biodegraded nanotubes do not generate an inflammatory response when aspirated into the lungs of mice. Our findings suggest that the extent to which carbon nanotubes are biodegraded may be a major determinant of the scale and severity of the associated inflammatory responses in exposed individuals.

The presence of engineered nanomaterials in technological applications and consumer products has raised concerns about their possible adverse effects on human health and the environment[2]. The unique physicochemical characteristics of carbon nanotubes make their biological effects largely unpredictable[3]. *In vitro* data indicate that single-walled carbon nanotubes may be cytotoxic, largely by inducing oxidative stress[4–6]. Mice exposed to nanotubes by aspiration or inhalation develop a robust pulmonary inflammatory response[7–9]. Inflammation has also been observed when multiwalled carbon nanotubes were injected intraperitoneally in mice[10].

The chemical degradation of pristine single-walled carbon nanotubes uses strong acids and oxidants (such as mixtures of sulphuric acid and hydrogen peroxide) to modify the surfaces of the nanotubes[11] and to cut them into shorter carboxylated nanotubes. Hypochlorite is also known to generate carboxyl and hydroxyl groups on nanotube surfaces[12,13], suggesting that strong oxidants may be effective in degrading nanotubes. However, the biodegradation routes of these nanomaterials remain unknown.

Neutrophils kill invading microorganisms by using their oxidantgenerating enzymes, such as nicotinamide adenine dinucleotide phosphate-oxidase (NADPH oxidase), myeloperoxidase and proteases[14]. Human myeloperoxidase (hMPO) generates potent reactive radical intermediates and hypochlorous acid (HOCl), which probably contribute to the degradation of implantable polymeric materials such as poly(ester-urea-urethane)[15]. We reasoned that these same potent hMPO oxidants could also biodegrade nanotubes.

We prepared short carboxylated single-walled carbon nanotubes by chemical cutting[11] (short-cut nanotubes) and used them throughout the study unless specified otherwise. On incubation with hMPO and H_2O_2, the nanotubes degraded over time, and the suspension turned translucent after 24 h (Fig. 1a). Neither hMPO alone nor H_2O_2 alone caused nanotube degradation. Incubation of hMPO with nanotubes alone, without H_2O_2, did not inactivate the enzyme (Supplementary Fig. S1a). In the presence of H_2O_2, however, hMPO retained 50% of its activity over 2.5 h but decayed after 5 h (Supplementary Fig. S1b). We therefore added fresh hMPO and H_2O_2 to the nanotube suspensions every 5 h.

Dynamic light scattering of nanotubes treated with hMPO and H_2O_2 showed several peaks that corresponded with a reduction in the size of the treated nanotubes compared to untreated controls (Fig. 1b). Native agarose gel electrophoresis showed that the majority of non-degraded carbon nanotubes remained as a dark congested band in the loading well or migrated as a smear in the presence of albumin/bromophenol blue. In contrast, no detectable bands were found on native gels when biodegraded carbon nanotubes were electrophoresed under similar conditions (Supplementary Fig. S1d). Furthermore, visible–near infrared (vis–

NIR) absorbance spectra of treated nanotubes showed that the characteristic metallic band (M1) and semiconducting (S2) transition band were suppressed during incubation (Fig. 1c). The disorder-induced D-band at ~1,250–1,350 cm^{-1} increased in the Raman spectra, whereas the tangential-mode G-band decreased with incubation time, suggesting that the graphene sidewall was oxidized (Fig. 1d). Drastic changes in nanotube morphology were further confirmed by transmission (TEM) and scanning electron microscopy (SEM). The characteristic fibrillar structure of intact nanotubes was completely lost, and the bulk of the nanotubes was no longer present after 24 h of incubation (Fig. 1e,f). Only a few visual fields showed evidence of residual carbonaceous material (Supplementary Fig. S1c).

After 12 h of incubation of the nanotubes with hMPO and H_2O_2, gas chromatography–mass spectrometry (GC–MS) revealed several major products, including short-chain tri-carboxylated alkanes and alkenes, and molecular ions of di-carboxylated short-chain and mono-carboxylated products (Supplementary Fig. S2). Analysis of the products extracted from fully biodegraded nanotubes demonstrated the presence of short-chain carboxylated alkanes and alkenes (data not shown). These results are in agreement with previous studies showing carboxylation of nanotubes on acid treatment[16]. Furthermore, a 60% increase in CO_2 levels was detected in biodegraded nanotubes compared to nanotubes incubated with hMPO alone or H_2O_2 alone.

Reactive radical intermediates of hMPO and hypochlorite could be two oxidants involved in nanotube biodegradation[17]. Both are formed when hMPO is incubated with H_2O_2 in the presence of sodium chloride (NaCl), whereas only peroxidase reactive radical intermediates are generated in the absence of NaCl. Biodegradation of nanotubes occurred during their incubation with hMPO and H_2O_2 in the absence of NaCl, although it was markedly suppressed compared to results obtained for incubation with hMPO and H_2O_2 plus NaCl (Supplementary Fig. S3). Accordingly, when nanotubes were exposed to sodium hypochlorite alone, the degradation process was markedly attenuated (Fig. 1a,b,e,f), suggesting a radical-driven mechanism. Taurine, a scavenger of HOCl (ref. 18), also impeded the biodegradation of nanotubes. The effect was similar to that achieved in a NaCl-free medium (Supplementary Fig. S3). Overall, these data imply that both the peroxidase reactive intermediates and hypochlorite contributed to biodegradation.

hMPO is known to avidly bind to negatively charged molecules, including an anionic phospholipid, phosphatidylserine (PS; ref. 19). PS-coated nanotubes showed biodegradation by hMPO, whereas nanotubes coated with non-charged phosphatidylcholine—a major lung surfactant phospholipid—were not biodegraded (Supplementary Fig. S4). To better understand the role of surface charges on short-cut nanotubes in the interactions with hMPO, we used molecular modelling. The simulations revealed two potential interaction sites between hMPO and the nanotubes. One site was located at the proximal end of the haem group, involving tyrosine residues 293 and 313 (known to be catalytically active in hMPO[20]; Fig. 2a, left). The simulation pointed to a strong interaction of positively charged residues on hMPO (Supplementary Table S1) with the carboxyl surface of the nanotubes, in line with studies performed by Kam and colleagues[21] on nanotube interactions with other proteins. We thus propose a site-localized reaction in which hMPO positive charges favour the binding of nanotubes, and radical-supporting aromatic groups participate in the cleavage of

the nanotubes (Supplementary Fig. S5). Atomic force microscopy demonstrated the attachment of hMPO to the surface of the nanotubes (Fig. 2d; Supplementary Fig. S6).

The second binding site close to the distal end of the haem group, far away from catalytically competent tyrosine residues 293 and 313 (Fig. 2a, right), may be involved in the binding of pristine (non-carboxylated) nanotubes. Notably, pristine nanotubes underwent less effective biodegradation by hMPO both in the presence and absence of NaCl (Supplementary Fig. S7). Pristine nanotubes have been shown to be susceptible to HOCl oxidation[13]. In line with this, our Raman spectroscopy data confirmed that the oxidation of pristine nanotubes is mediated by hypochlorite (Supplementary Fig. S8). Interestingly, the short-cut nanotubes were equally susceptible to oxidation, indicating a random reaction of hypochlorite with both types of nanotubes. It is tempting to speculate that HOCl might be essential for triggering and initially accumulating carboxylated sites on pristine nanotubes, which leads to the better positioning of hMPO and subsequent biodegradation of the tubes by reactive intermediates of the enzyme (Fig. 2).

We next evaluated whether oxidative biodegradation of nanotubes can be executed by hMPO-rich human neutrophils. Stimulation of neutrophils was performed using a chemoattractant, N-formyl-methionylleucyl-phenylalanine (fMLP), in combination with a degranulation promoting agent, cytochalasin B. Cytochalasin B is known to increase the activity of hMPO and trigger its release[22]. During neutrophil activation, hMPO is translocated into phagosomes, in which the fully assembled, membrane-bound NADPH oxidase generates superoxide radicals[14]. The latter dismutates to H_2O_2, which enables hMPO to produce reactive intermediates and HOCl. Dihydroethidium staining and cytochrome-c reduction assay confirmed the activation of neutrophils on stimulation with fMLP and cytochalasin B (Fig. 3a,b). Because 75% of the total hMPO remained inside the cells (Fig. 3c), we targeted nanotubes to neutrophils by using IgG functionalization[23]. Using fluorescently labelled nanotubes, we found a significant increase in the uptake of IgG–nanotubes by neutrophils compared to that of nonfunctionalized nanotubes (Supplementary Fig. S9a,b). Furthermore, we observed sustained basal generation of oxidants (for up to 12 h) by neutrophils incubated with IgG–nanotubes as assessed by $2',7'$ dichlorofluorescein-di-acetate and Amplex Red assays (Fig. 3d; Supplementary Fig. S10).

Under these conditions, IgG–nanotubes underwent 100% degradation, whereas only 30% of non-IgG-functionalized nanotubes were degraded in neutrophil suspensions, as was made evident by infrared spectroscopy (Fig. 4a). Inhibitors of hMPO (4-aminobenzoic acid hydrazide)[24] and NADPH oxidase (apocynin)[25] attenuated the degradation process (Supplementary Fig. S11). This finding suggests that both hMPO and NADPH oxidase were essential for nanotube biodegradation by neutrophils. Raman microscopy of IgG-functionalized nanotubes inside neutrophils showed a marked loss of the G-band and appearance of a strong D-band. This is characteristic of oxidatively modified nanotubes (Fig. 4b,c) and demonstrates that the uptake of IgG-functionalized nanotubes by neutrophils resulted in an hMPO-driven biodegradation process in activated cells.

Human monocyte derived macrophages are known to contain lower levels of hMPO than neutrophils (13 ng hMPO per 10^6 macrophages, compared with 1.8 μg hMPO per 10^6

neutrophils). Infrared spectroscopic assessments revealed only negligible degradation of IgG–nanotubes by macrophages after 6 h of incubation and 13% degradation at 12 h (compared with 30% and 100% biodegradation of IgG–nanotubes by neutrophils at 6 and 12 h, respectively; Supplementary Fig. S11). More pronounced (~50%) biodegradation of IgG–nanotubes by macrophages occurred only after 48 h. As described previously[26,27], these results suggest that hMPO activity is an important determinant of the biodegradation of nanotubes as well as other nanoformulations.

Pharyngeal aspiration or inhalation of nanotubes is known to induce a robust pulmonary inflammatory response in mice, with early onset of fibrosis[7,8]. To address whether the biodegradation process would render nanotubes non-inflammatory, we assessed the amounts of neutrophils and the levels of cytokines in broncheoalveolar lavage obtained from mice at day 1 (Fig. 5a) and day 7 (Supplementary Fig. S12) after nanotube exposure. The profiles of these inflammation markers in animals exposed to biodegraded nanotubes by pharyngeal aspiration were essentially indistinguishable from control values. In contrast, non-degraded short-cut nanotubes elicited an acute inflammatory response. Similar responses were seen with nanotubes pre-incubated with either hMPO or H_2O_2 alone (Fig. 5a). Non-degraded nanotubes also induced the formation of tissue granulomas, but no granulomas were observed in the lungs of mice exposed to biodegraded nanotubes (Fig. 5b).

Partially degraded nanotubes obtained after 12 h of incubation with hMPO and H_2O_2 still retained some of their characteristic morphologic and spectral features, and induced less inflammation in mice than the non-biodegraded nanotubes (Supplementary Fig. S13). Thus, hMPO-mediated biodegradation of nanotubes serves to mitigate the pro-inflammatory potential of these nanomaterials.

To summarize, we have shown a novel route of enzymatic biodegradation of single-walled carbon nanotubes relevant to potential respiratory exposures during the production and handling of carbon nanotubes. Based on these findings, strategies for mitigating the pro-inflammatory effects of these nanomaterials in the occupational setting may be developed. Pulmonary inflammation following carbon nanotube exposures in mice[7–9] could be explained by the ineffective internalization of non-functionalized nanotubes by phagocytic cells[28]. Moreover, it is possible that the doses of nanotubes commonly used in toxicological studies may overwhelm the biodegradation capacity of the neutrophil enzymatic system. Nonetheless, the propensity of nanotubes to undergo hMPO-mediated biodegradation suggests that these nanomaterials may be considered as tools for delivery of therapeutic agents in biomedical applications when used at appropriate and readily degradable concentrations.

Methods

Degradation of nanotubes

Mixtures contained 30 μg hMPO with an activity of 1.1 U μg^{-1} (Sigma) per 300 μg of nanotubes suspended in 300 μl of 50 mM phosphate buffer containing 140 mM NaCl and 100 μM diethylene triamine pentaacetic acid (DTPA), a transition metal chelator. Hydrogen peroxide was added at a rate of 200 μM per hour for 5 h. Because of loss of activity of

hMPO in the incubation system, the enzyme was replenished after 5 h and the reaction mixture was maintained at 37 °C for 24 h. Where indicated, sodium hypochlorite was added every hour to give concentrations of 200 μM for 24 h at 37 °C.

Computational modelling

The three-dimensional structures of nanotubes were generated using Nanotube Modeller software (http://www.jcrystal.com/products/wincnt/index.htm). The diameter was set at 1.1 nm using chirality parameters m and n of 14 and 0. For carboxylated nanotubes, one of the ends of the nanotube was carboxylated using the Builder tool, provided by Pymol[29] visualization software. Nanotubes were docked to the hMPO X-ray crystal structure (PDB ID: 1CXP, chains A & C), using the Lamarckian Genetic Algorithm provided by AutoDock4.0 software, as described previously[30] with the following modifications. The entire surface of the target was searched for possible binding sites without bias. The grid maps representing the protein were calculated using the AutoGrid option. A cubic box was built around the protein with $126 \times 126 \times 126$ points. A spacing of 0.41 Å between the grid points was used, placing the centre of the protein at the centre of the cube. Docking simulations were carried out with an initial population of 300 structures, and a maximum number of 50,000,000 energy evaluations. The resulting top 25 minimum energy orientations with 2.0 Å r.m.s. deviation were clustered. AutoDock4.0 software was run using distributed computing (www.pittgrid.pitt.edu).

Functionalized nanotubes with IgG

Nanotubes (200 μg) in HEPES buffer (pH 7.4) were incubated with purified human IgG (Invitrogen) in 1:1 ratio (w/w) for 48 h at 37 °C with sonication for 10 min every 5 h in a water bath sonicator.

Raman microscopy of nanotubes in neutrophils

Cells incubated with IgG– nanotubes were fixed using 2.5% paraformaldehyde and cyto-spun onto 1.5-mmthick cover glass (Fisher Scientific). An NTEGRA SPECTRA AFM–Raman microscope (NT-MDT) was used with a cobalt solid-state laser operating at a wavelength of 473 nm. All Raman spectra were recorded for 2 s, at 10% laser power, using a ×100 oil immersion objective. For each spectrum a static grating (2,400 l mm^{-1}) scan was taken over the range 678.28–2,231.82 cm^{-1}. Detection of the Raman scattered light was performed using a Peltier cooled charge-coupled device detector. From each of the samples an average of 20 spectra was recorded.

hMPO contents in cells and its release

Levels of hMPO in cells were determined by ELISA kit (Alpco Diagnostics) after 30 min incubation with either fMLP with cytochalasin B or nanotubes. Neutrophils were centrifuged at 1,000g for 10 min. The supernatant and pellet were obtained and used separately for hMPO measurements according to the manufacturer's manual. The amounts of hMPO were expressed as ng/10^6 cells.

Infrared spectroscopy of nanotubes in neutrophils

Neutrophils incubated with IgG–nanotubes were harvested from culture plates after 24 h of incubation together with the incubation medium. The cell suspensions were further subjected to harsh sonication for 1 h using the ultrasonic probe tip sonicator (Cole-Palmer Ultrasonic Homogenizer, 20 kHz), and the spectra were then recorded in the samples using a vis–NIR spectrophotometer (Perkin-Elmer).

Particulate instillation

Pharyngeal aspiration was used for particulate administration to C57BL/6 mice. Briefly, after anaesthetization with ketamine and xylazine anesthesia (62.5 and 2.5 mg kg^{-1}, respectively), the mouse was placed on a board in a near-vertical position. The animal's tongue was extended with lined forceps, and a suspension of particulates (50 μl, non-biodegraded and biodegraded nanotubes at a dose of 40 μg/mouse each) was placed in the posterior of pharynx. The tongue was held until the suspension was aspirated into the lungs. All mice in particle and phosphate buffered saline control groups survived this exposure procedure. This technique provides a good distribution of particles, widely disseminated in a peri-bronchiolar pattern within the alveolar region. Animals treated with the particulates recovered easily after anaesthesia with no behavioural or negative health outcomes.

Supplementary Material

Refer to Web version on PubMed Central for supplementary material.

Acknowledgements

References

1. Allen BL et al. Biodegradation of single-walled carbon nanotubes through enzymatic catalysis. Nano Lett. 8, 3899–3903 (2008). [PubMed: 18954125]

2. Maynard AD et al. Safe handling of nanotechnology. Nature 444, 267–269 (2006). [PubMed: 17108940]

3. Shvedova AA et al. Mechanisms of pulmonary toxicity and medical applications of carbon nanotubes: two faces of Janus? Pharmacol. Ther 121, 192–204 (2009). [PubMed: 19103221]

4. Jia G et al. Cytotoxicity of carbon nanomaterials: single-wall nanotube, multi-wall nanotube and fullerene. Environ. Sci. Technol 39, 1378–1383 (2005). [PubMed: 15787380]

5. Kagan VE et al. Direct and indirect effects of single walled carbon nanotubes on RAW 264.7 macrophages: role of iron. Toxicol. Lett 165, 88–100 (2006). [PubMed: 16527436]

6. Kisin ER et al. Single-walled carbon nanotubes: geno- and cytotoxic effects in lung fibroblast V79 cells. J. Toxicol. Environ. Health. A 70, 2071–2079 (2007). [PubMed: 18049996]

7. Shvedova AA et al. Unusual inflammatory and fibrogenic pulmonary responses to single-walled carbon nanotubes in mice. Am. J. Physiol. Lung Cell. Mol. Physiol 289, L698–L708 (2005). [PubMed: 15951334]

8. Shvedova AA et al. Inhalation vs. aspiration of single-walled carbon nanotubes in C57BL/6 mice: inflammation, fibrosis, oxidative stress and mutagenesis. Am. J. Physiol. Lung Cell. Mol. Physiol 295, L552–L565 (2008). [PubMed: 18658273]

9. Muller J et al. Structural defects play a major role in the acute lung toxicity of multiwall carbon nanotubes: toxicological aspects. Chem. Res. Toxicol 21, 1698–1705 (2008). [PubMed: 18636756]

10. Poland CA et al. Carbon nanotubes introduced into the abdominal cavity of mice show asbestos-like pathogenicity in a pilot study. Nature Nanotech. 3, 423–428 (2008).

11. Wei Z, Kondratenko M, Dao LH & Perepichka DF Rectifying diodes from asymmetrically functionalized single-wall carbon nanotubes. J. Am. Chem. Soc 128, 3134–3135 (2006). [PubMed: 16522080]

12. Yoon SM et al. Selective oxidation on metallic carbon nanotubes by halogen oxoanions. J. Am. Chem. Soc 130, 2610–2616 (2008). [PubMed: 18251473]

13. Wu CH Studies of the equilibrium and thermodynamics of the absorption of Cu^{2+} onto as-produced and modified carbon nanotubes. J. Colloid Interface Sci 311, 338–346 (2007). [PubMed: 17442333]

14. Hampton MB, Kettle AJ & Winterbourn CC Inside the neutrophil phagosome: oxidants, myeloperoxidase and bacterial killing. Blood 92, 3007–3017 (1998). [PubMed: 9787133]

15. Sutherland K, Mahoney JR II, Coury AJ & Eaton JW Degradation of biomaterials by phagocyte-derived oxidants. J. Clin. Invest 92, 2360–2367 (1993). [PubMed: 8227352]

16. Kuznetsova A et al. Oxygen-containing functional groups on single-wall carbon nanotubes: NEXAFS and vibrational spectroscopic studies. J. Am. Chem. Soc 123, 10699–10704 (2001). [PubMed: 11674002]

17. Panasenko OM et al. Generation of free radicals during decomposition of hydroperoxide in the presence of myeloperoxidase or activated neutrophils. Biochemistry (Mosc) 70, 998–1004 (2005). [PubMed: 16266270]

18. Kearns S & Dawson R Jr. Cytoprotective effect of taurine against hypochlorous acid toxicity to PC12 cells. Adv. Exp. Med. Biol 483, 563–570 (2000). [PubMed: 11787641]

19. Lessig J et al. Myeloperoxidase binds to non-vital spermatozoa on phosphatidylserine epitopes. Apoptosis 12, 1803–1812 (2007). [PubMed: 17701359]

20. Olivier ML & Paul RO EPR spin-trapping of a myeloperoxidase protein radical. Biochem. Biophys. Res. Commun 1, 199–202 (2000).

21. Kam N & Dai H Single walled carbon nantoubes for transport and delivery of biological cargos. Phys. Stat. Sol 243, 3561–3566 (2006).

22. Zipfel M, Carmine TC, Gerber C, Niethammer D & Bruchelt G Evidence for the activation of myeloperoxidase by f-Meth-Leu-Phe prior to its release from neutrophil granulocytes. Biochem. Biophys. Res. Commun 232, 209–212 (1997). [PubMed: 9125133]

23. McKenzie SE & Schreiber AD Fc gamma receptors in phagocytes. Curr. Opin. Hematol 5, 16–21 (1998). [PubMed: 9515197]

24. Kettle AJ, Gedye CA & Winterbourn CC Mechanism of inactivation of myeloperoxidase by 4-aminobenzoic acid hydrazide. Biochem. J 321, 503–508 (1997). [PubMed: 9020887]

25. Touyz RM Apocynin, NADPH oxidase and vascular cells: a complex matter. Hypertension 51, 172–174 (2008). [PubMed: 18086948]

26. Batrakova EV et al. A macrophage–nanozyme delivery system for Parkinson's disease. Bioconjug. Chem 18, 1498–1506 (2007). [PubMed: 17760417]

27. Dou H et al. Development of a macrophage-based nanoparticle platform for antiretroviral drug delivery. Blood 108, 2827–2835 (2006). [PubMed: 16809617]

28. Konduru NV et al. Phosphatidylserine targets single-walled carbon nanotubes to professional phagocytes *in vitro* and *in vivo*. PLoS One 4, e4398 (2009). [PubMed: 19198650]

29. DeLano WL The PyMOL Molecular Graphics System (DeLano Scientific, 2002).
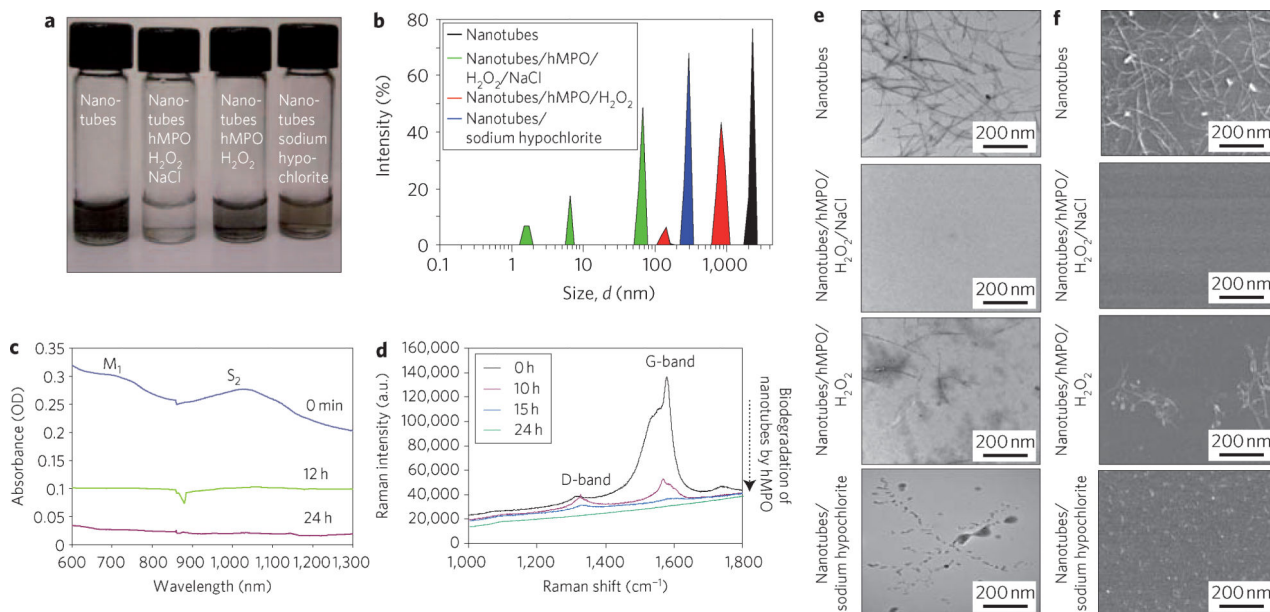
30. Yanamala N, Tirupula KC & Klein-Seetharaman J Preferential binding of allosteric modulators to active and inactive conformational states of metabotropic glutamate receptors. BMC Bioinformatics 9(Suppl 1), S16 (2008).

Figure 1 |. Spectroscopic and electron microscopic evaluation of human myeloperoxidase (hMPO)-mediated degradation of nanotubes *in vitro*.

a, Photograph of different short-cut nanotube suspensions after 24 h. **b,** Dynamic light scattering showing multiple smaller peaks corresponding to biodegraded nanotubes. **c,** Infrared spectra showing loss of M1 and S2 bands as nanotubes are degraded in the presence of hMPO and H_2O_2. OD, optical density. **d,** Raman spectra (excitation, 633 nm) of ethanol-dried nanotubes (black) and (hMPO and H_2O_2)-treated nanotubes, showing loss of the characteristic G-band, followed by appearance and decay of the D-band over time. **e,f,** TEM (**e**) and SEM (**f**) analyses, tracking the biodegradation of nanotubes after 24 h.
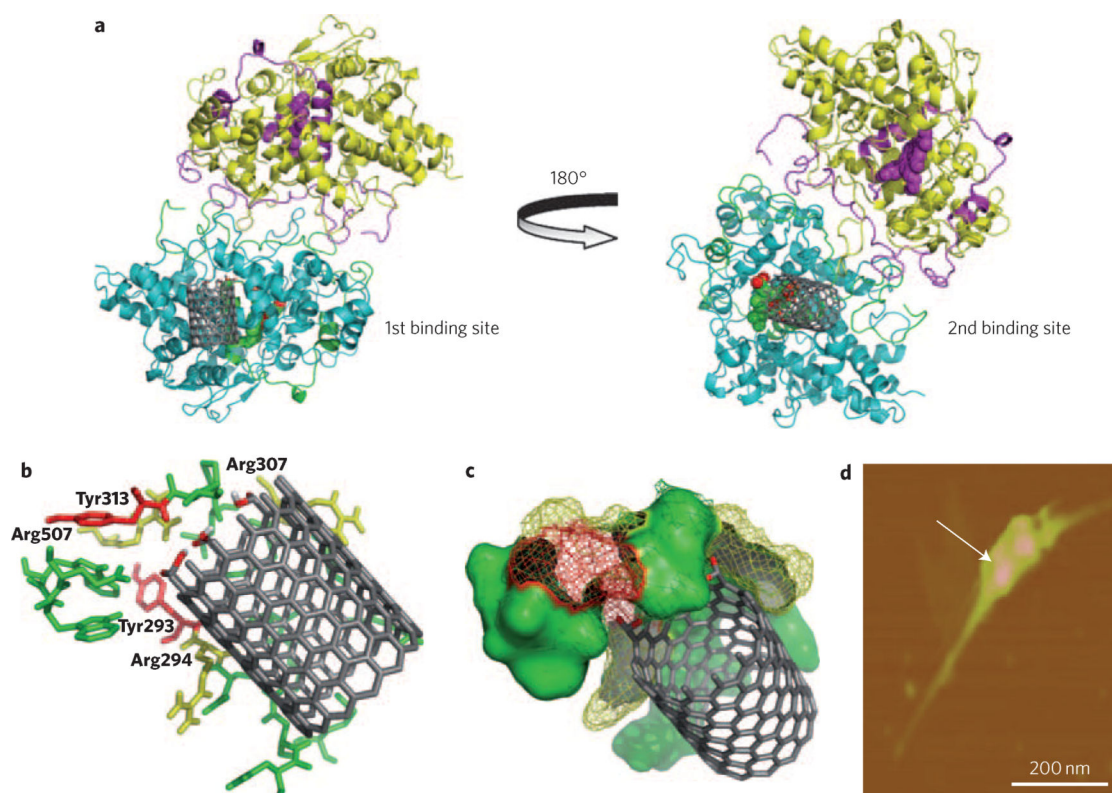
Figure 2 |. Molecular modelling, demonstrating possible nanotube interaction sites on hMPO.
a, Two putative binding sites for nanotubes on the hMPO monomer surface are located on each side of the protein. The best model site with lowest binding energy is shown for carboxylated short-cut nanotubes (left) and pristine nanotubes (right). **b,** Stabilization of the carboxylated ends of the nanotubes by arginine (yellow) and tyrosine residues (red) in hMPO in the first binding pocket (left). All residues shown are within 5 Å of nanotubes and are predicted to participate in the degradative catalysis of nanotubes. This includes Tyr293, Arg294, Arg307, Tyr313 and Arg507. **c,** As **b**, using space-fill representation. **d,** AFM image confirming the binding of a dimer of hMPO with a single nanotube.
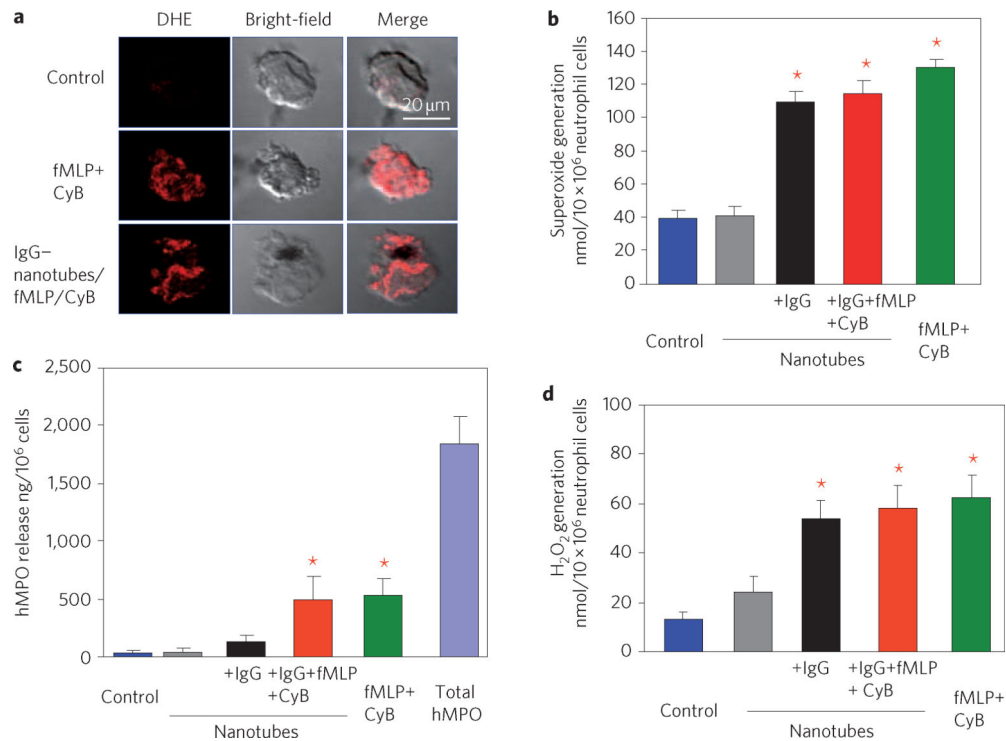
Figure 3 |. IgG-functionalized nanotubes induce the release of hMPO and the generation of reactive oxygen species in human peripheral blood neutrophils.
a, Assessments of intracellular superoxide in neutrophils treated with fMLP and cytochalasin B (CyB) alone or plus IgG–nanotubes for 30 min at 37 °C. Representative confocal micrographs of neutrophils stained with dihydroethidium (DHE) to detect superoxide generation are shown. **b**, Quantitative assessment of extracellular generation of superoxide radicals. **c**, Extracellular release of hMPO in response to fMLP, cytochalasin B and IgG–nanotubes. **d**, Generation of extracellular H_2O_2 30 min after challenge with nanotubes assessed by the Amplex red assay. Data shown in panels **b–d** are from three independent experiments performed with neutrophils obtained from different donors and are expressed as mean values±s.d. (*$P < 0.05$, groups versus control). Error bars in **b–d** represent standard deviations (s.d.).
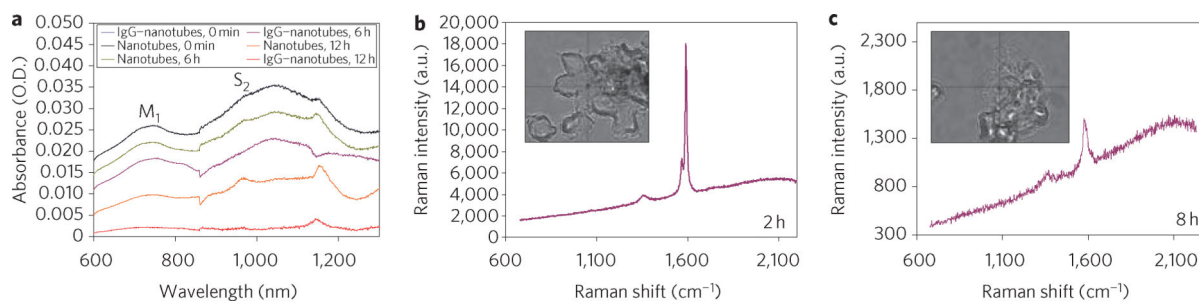
Figure 4 |. Biodegradation of nanotubes in neutrophils evaluated by infrared and Raman spectroscopy.

a, Vis–NIR spectra showing biodegradation of nanotubes and IgG–nanotubes by human neutrophils after 0, 6 and 12 h. O.D., optical density. **b,c,** Raman spectra (excitation, 473 nm) recorded from different areas of neutrophils containing IgG–nanotubes at 2 h (**b**) and 8 h (**c**). Inset shows bright-field image of the neutrophils with engulfed IgG–nanotubes. The Raman spectra (red lines) with their corresponding G- and D-bands recorded from different areas of neutrophils are indicated by the cross-wire on the bright-field images.
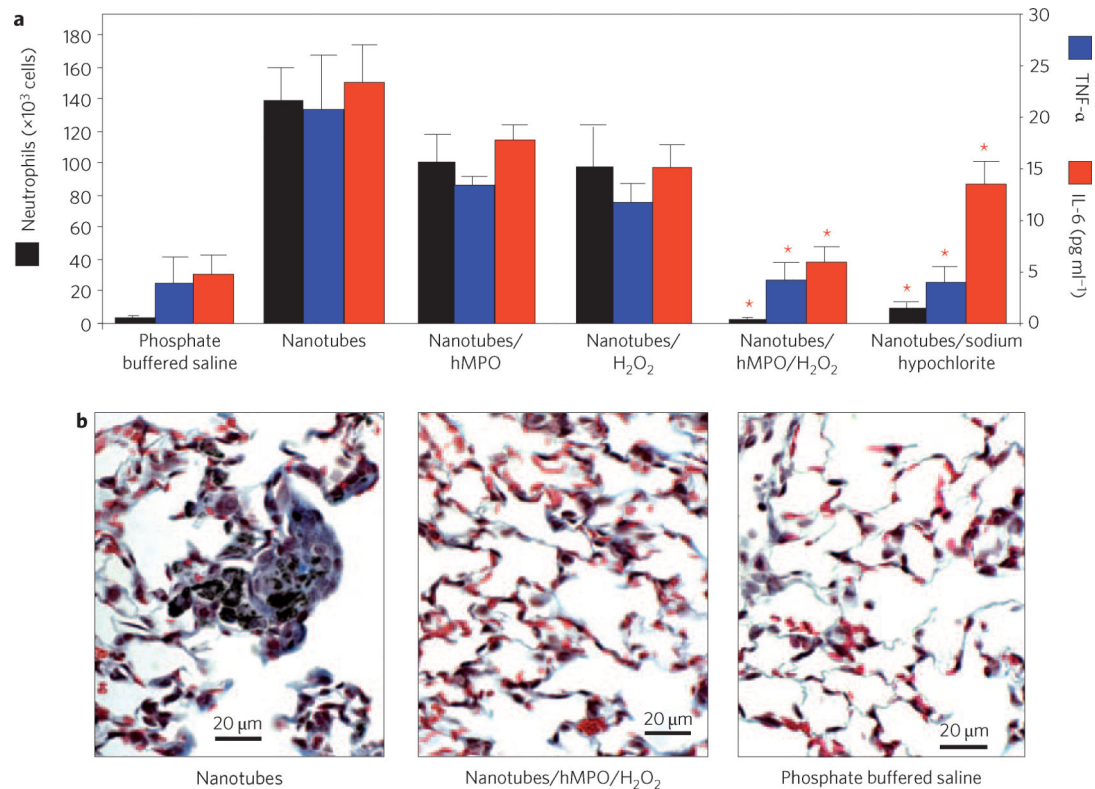
Figure 5 |. Biodegraded nanotubes do not elicit a pro-inflammatory pulmonary response in C57BL/6 mice.

a, Neutrophil counts and expression of TNF-α (blue) and IL-6 (red) in broncheoalveolar lavage fluid were measured 24 h after exposure to the indicated treatments by means of pharyngeal aspiration. Data represent mean values±s.e. ($n = 6$ mice per group). *$P < 0.05$ groups versus nanotubes alone. **b,** Representative images of lung sections from mice exposed to 40 μg/animal nanotubes, showing granuloma formation on day 7 after pharyngeal aspiration. Similar to the results from control animals exposed to phosphate buffered saline, no granuloma formation is seen in the lungs of mice exposed to degraded nanotubes. Biodegradation of nanotubes was induced by their incubation with hMPO and H_2O_2. Error bars in **a** represent standard error (s.e.).